Blade Element Momentum Theory (BEM) Assignment

AE4135 Rotor / Wake Aerodynamics

by

Group 21

Chirag Bansal (6137776)
Ninad Gajanan (6272053)
Tanmay Gupta (6170455)

Instructor:	Dr. Wei Yu
Faculty:	Faculty of Aerospace Engineering, Delft
Date:	March 25, 2025

Contents

1 Introduction

1.1 Blade Element Momentum Theory

Blade Element Momentum (BEM) theory combines two aerodynamic theories: momentum theory and blade element theory. Together, they give us a practical and accurate approximation to predict rotor performance.

Momentum theory treats the rotor as an actuator disk that pushes air down to create thrust. It uses the governing conservation laws: mass, momentum, and energy, to approximate how fast the air has to move to generate a certain amount of thrust and power. But a limitation is that it assumes the force is spread evenly across the rotor disk, which isn't accurate in real life.

While in Blade element theory, it slices the blade into small sections and calculates the lift and drag on each one based on airfoil data. This way, it takes into account how wind speed and angle change along the blade's length. The limitation here is that it doesn't consider how one part of the blade affects another, or how the rotor's wake influences things.

The blade element momentum theory equates the thrust from the blade element theory and the actuator disk momentum theory. This allows for the calculation of the induction factor. BEM uses an iterative process to solve for the induction factor which is explained in detail in section 2. The iteratively solved induction factors allows for computing different aerodynamic parameters at different parts of the blade. Corrections are applied like Prandtl tip and root correction, which account for the effects near the blade tips and root, leading to more accurate results. Although the assumptions applied to this theory (section 3) limit its applicability, it gives a good approximation for preliminary design.

1.2 Case Setup: Propeller Analysis

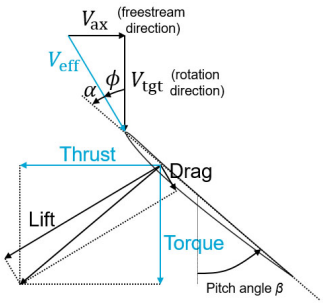

Figure 1: Propeller blade force decomposition.

This assignment focuses on implementing a BEM model to analyze a propeller operating in axial flow. The propeller has a radius, $R = 0.70$ m, 6 blades, and features the ARA-D8% airfoil. Performance will be evaluated at Advance ratios of $J \in \{1.6, 2.0, 2.4\}$. The propeller operates at $V_\infty = 60$ m/s, and an altitude of $h = 2000$ m under standard atmospheric conditions.

Using the BEM framework, we will compute key aerodynamic parameters such as thrust, torque, power, and induced flow characteristics. Additionally, we will assess the impact of aerodynamic corrections and evaluate the sensitivity of the results to different advance ratios. This analysis will provide insights into the effectiveness of BEM theory for modeling propeller aerodynamics.

2 Flowchart

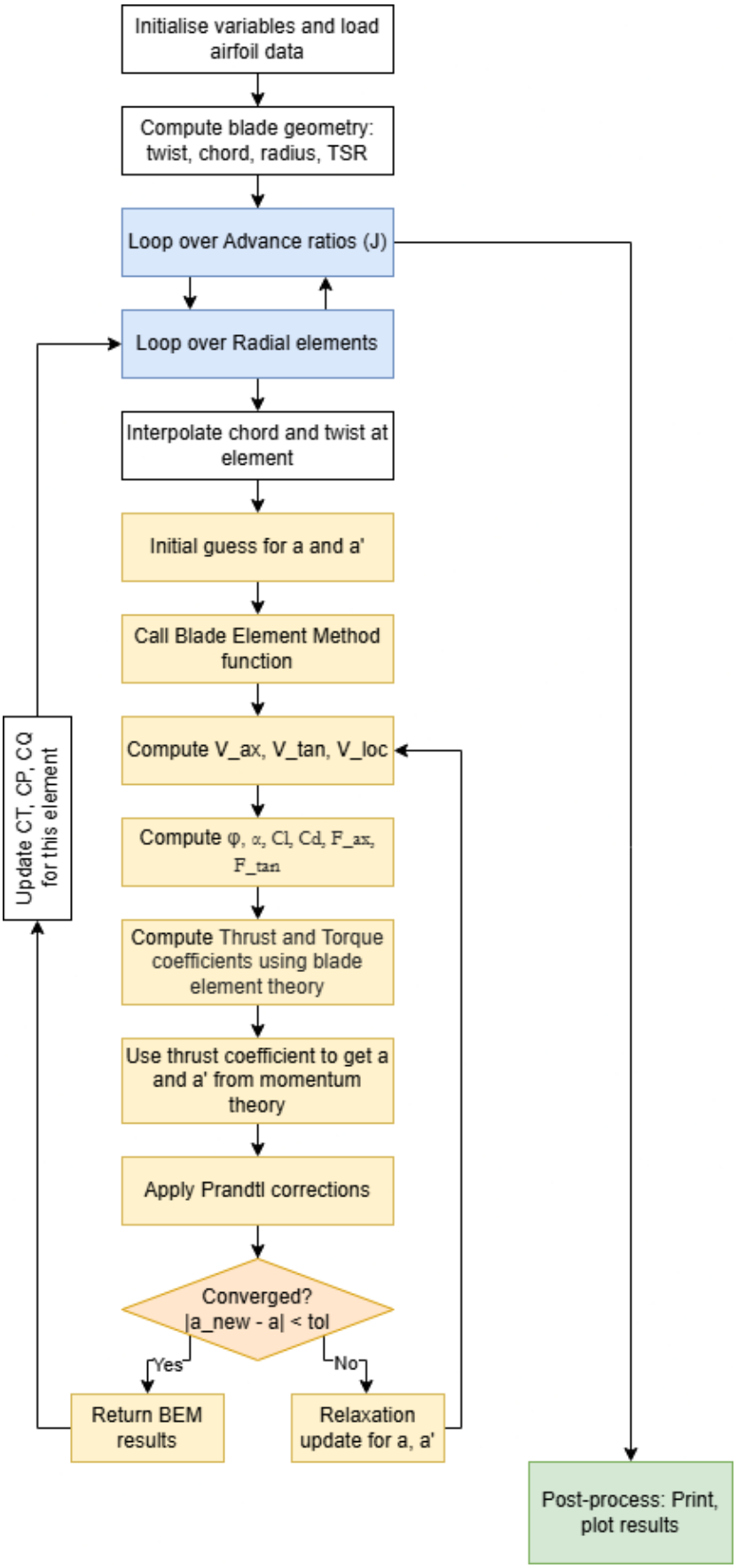

Figure 2: Flowchart for BEM Code

3 Assumptions

Various assumptions were made while designing the Blade Element Momentum model which are listed below:

- The rotor blade is discretized into annular rings of infinitesimally small thickness. This is done so that it can be assumed that there is no interaction between annular rings of different blades. This assumption simplifies the problem to avoid the complex 3D effects of tip vortices and their interactions. This limits the accuracy of the BEM model.
- The BEM model assumes that the global force on the actuator disk equals the local forces on the blades.
- The flow is assumed to be inviscid. Viscous effects cannot be taken into account in the BEM model that is used for this assignment.
- The flow is assumed to be steady. Here, the time derivatives of the conservation equations can be neglected. In reality, there are unsteady effect due to turbulence which this BEM model cannot account for.
- The flow is assumed to be incompressible and isentropic. So for high Mach number flows, the model would not accurately predict the aerodynamic parameters, which is often the case for propellers used in large transport aircraft.
- The model assumes that there is a uniform distribution of loading over the actuator disk. This implies that it assumes there are an infinite number of blades. A finite number of blades causes a concentration of loading on the blades and vortex shedding at the tip and root of each blade. To account for this, a correction is used which is explained further in subsection 4.5.
- The model assumes no radial flow over the blades. This makes the model inaccurate in heavily loaded cases. However, since this model is developed for propellers, this assumption is within reason.
- The model assumes that 2D airfoil properties can be applied without taking into account the 3D effects.

4 Results

4.1 Spanwise distribution of angle of attack and inflow angle

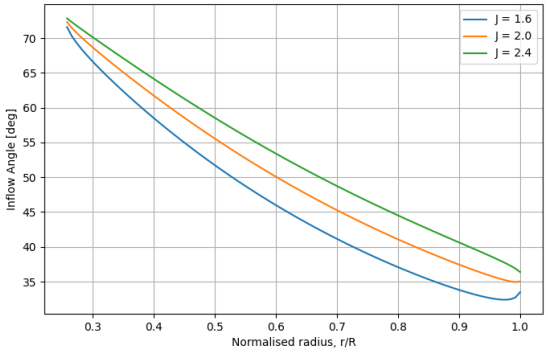

Figure 3: Inflow angle across blade radius

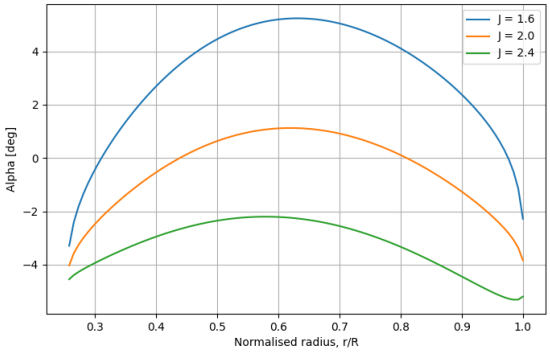

Figure 4: Angle of attack across blade radius

The inflow angles experienced by each blade element are guided by the tangential (V_{tan}), and axial (V_{ax}) velocities as given by Equation 1. High inflow angles are experienced at the root of the blade due to low tangential component of local velocity, and this value decreases along the span as V_{tan} increases. The blade twist, β, and inflow angle, ϕ influence the blade element angle of attack, α, given by Equation 2. Highest α, is experienced between $60-70\%$ of the rotor blade. This is due to the geometric definition of the propeller blade.

$$\phi = \arctan \frac{V_{ax}}{V_{tan}} \tag{1}$$

$$\alpha = \beta - \phi \tag{2}$$

4.2 Spanwise distribution of axial and azimuthal inductions

Induction is defined as the change in the wind speed due to the presence of the rotor (represented as an actuator disk). The axial induction factor is the change in wind speed in the direction of the axis of the propeller. For a propeller, there is an increase in the wind speed at the rotor. The axial induction factor is given by

$$a = \frac{V_{axial(rotor)} - V_{inf}}{V_{inf}} \tag{3}$$

It can be observed from Figure 5 that the values of the axial induction factor does not exceed 0.2 anywhere across the blade span. These results are consistent with theory, since propellers do not experience heavy loading. At the tip, there is an increase in the axial induction due to concentrated tip vortex shedding (see subsection 4.5 for more details). At higher advance ratios, the value of the axial induction factor decreases overall which shows agreeable results since higher advance ratios indicated a lower thrust coefficient, which indicates that the flow is comparatively less accelerated.

Figure 6 shows the variation of the tangential induction factor across the blade span. The tangential induction factor is given by

$$a' = 1 - \frac{V_{tan(rotor)}}{\omega r} \tag{4}$$

At the root, the tangential induction factor increases due to Prandtl corrections(see subsection 4.5). As the advanced ratio increases, it implies that the rotational velocity decreases, which decreases the tangential induction factor(see Equation 4).

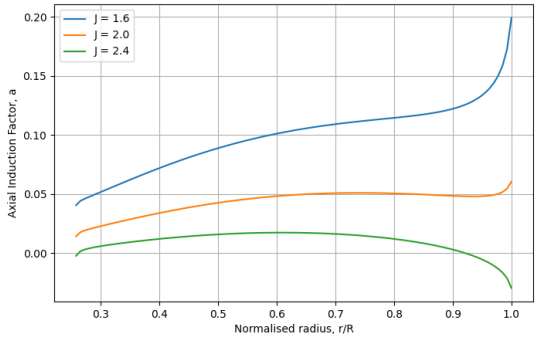

Figure 5: Axial induction factor across blade radius

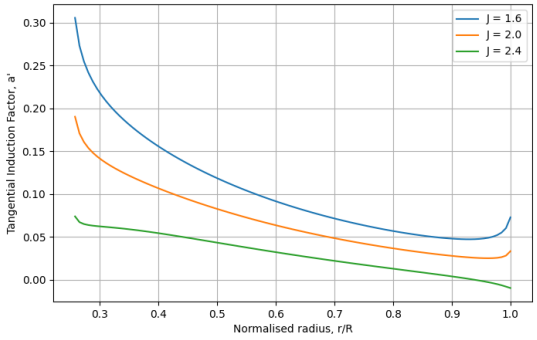

Figure 6: Tangential induction factor across blade radius

4.3 Spanwise distribution of thrust and azimuthal loading

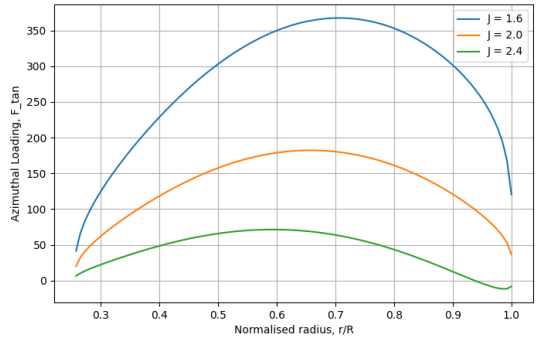

Figure 7: Azimuthal Loading across blade radius

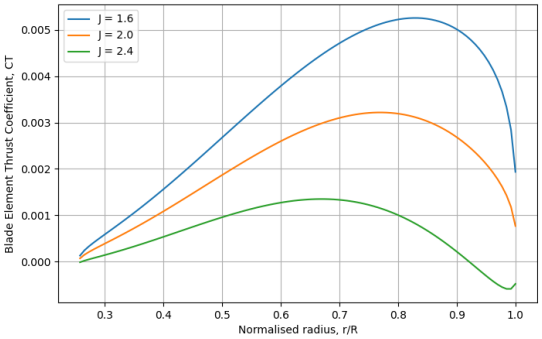

Figure 8: Thrust Coefficient across blade radius

Variation in thrust of each blade element is observed along the span of the blade as well as for different advance ratios. The advance ratio directly affects rotational speed of each blade element. As a result, the angle of attack experienced by each element is inherently different. Due to the variation in α, the load distribution on blade is also affected. Since thrust generated by the blade is majorly dependent on lift generated by each element (see Equation 5), the thrust distribution also changes. Increase in J, reduces the thrust generated as sectional lift is reduced due to lower local α.

$$dCT = \frac{0.5\rho V_{eff}^2 (C_l \sin\phi - C_d \cos\phi) c N_b dr}{\rho n^2 D^4} \tag{5}$$

$$dCQ = \frac{0.5\rho V_{eff}^2 (C_l \sin\phi + C_d \cos\phi) c N_b r dr}{\rho n^2 D^5} \tag{6}$$

Azimuthal loading increases along the span as the radial distance from the hub increases, which increases the rotational speed of the blade element. Trends similar to thrust are observed and can be attributed to lower rotational speeds due to increase in J (see Equation 7). Increase in J, decreases the tip-speed ratio, λ and inherently reduces the azimuthal forces on the blade.

$$J = \frac{V_{inf}}{nD} = \frac{\pi}{\lambda} \tag{7}$$

4.4 Variation of thrust and torque with advance ratio

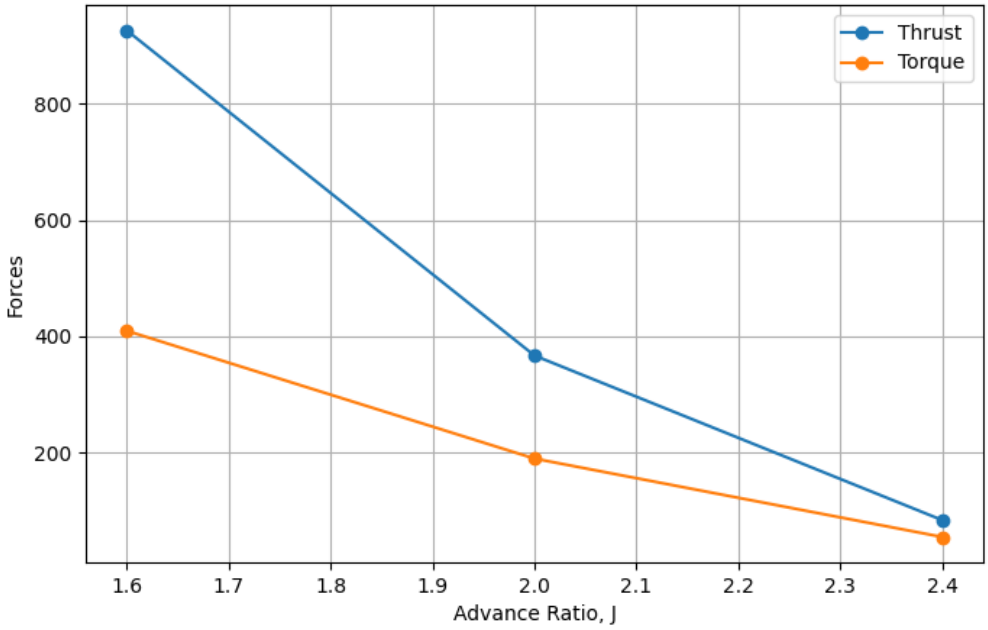

Figure 9: Thrust and Torque vs Advance Ratio

Thrust variations for different advance ratios has been addressed in section subsection 4.3. As for the torque generated by the rotor, similar line of reasoning can be adopted to explain the effects. Increasing the advance ratio, decreases the loading on each blade element, as a result, the torque generated is also lower (see Equation 6).

4.5 Effect of Prandtl Correction on the induction factor

The blade element momentum theory assumes that there is a uniform distribution of loading across the entire actuator disk. This implies that the original theory considers that there are an infinite number of blades. This simplification assumes that there is uniform flow at the propeller and the wake will be cylindrical in shape. However, in reality, there are finite number of blades (in the current case, 6). This will alter the flowfield significantly, since there will be an interaction of the flow particles with the blades, and the wake will have a helical screw-like structure. Further, a finite number of blades cause a concentration of loading at the blades, and there is a concentration of vortices at the root and tip, which results in vortex shedding. These concentrated vortices cause an increase in the induction at these locations. This effect needs to be corrected to have an accurate prediction of the flow field. Prandtl correction is used to increase the induction at the root and tip. The correction is given by Equation 8, Equation 9, and Equation 10.

$$f_{tip} = \frac{2}{\pi} arccos\left(e^{-\frac{B}{2}\left(\frac{1-\mu}{\mu}\right)\sqrt{1+\frac{\lambda^2\mu^2}{(1+a)^2}}} \right) \tag{8}$$

$$f_{root} = \frac{2}{\pi} arccos\left(e^{-\frac{B}{2}\left(\frac{\mu-\mu_{root}}{\mu}\right)\sqrt{1+\frac{\lambda^2\mu^2}{(1+a)^2}}} \right) \tag{9}$$

$$f_{total} = f_{tip} \times f_{root} \tag{10}$$

The tip and root corrections are given in Equation 8 and Equation 9. The corrections are dependent on the number of blades(B), the radial location($\mu = r/R$), the tip speed ratio(λ) and the induction factor(a). μ_{root} is the location of the root vortex.

The tip and root effects are combined to give a total correction given in Equation 10. The Prandtl correction factor is plotted across the blade radius in Figure 10. It can be seen that the corrections are majorly applied in the root and tip regions and in the mid sections, the correction factor is close to 1.

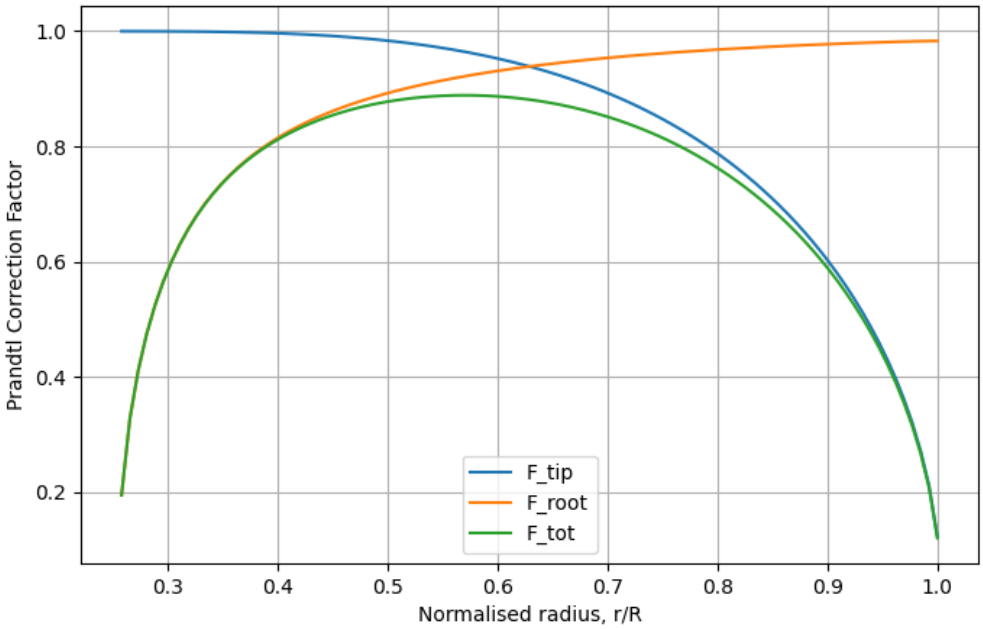

Figure 10: Prandtl tip and root correction

The Prandtl correction is applied to the axial induction factor(a) and tangential induction factor(a') in the following way:

$$a = a/f_{total} \tag{11}$$

$$a' = a'/f_{total} \tag{12}$$

To understand how the Prandtl correction factor affects the induction factor, the axial induction factor is plotted before and after correction in Figure 11 and Figure 12. It can be seen that before the corrections, the root and tip induction is very low. At the tip, the after-correction induction can be

seen to be prominent. This is because the induction factor value before the correction was significant. However, at the root, the induction factor was insignificant. Hence even after corrections, there is only a minor increase in the induction factor.

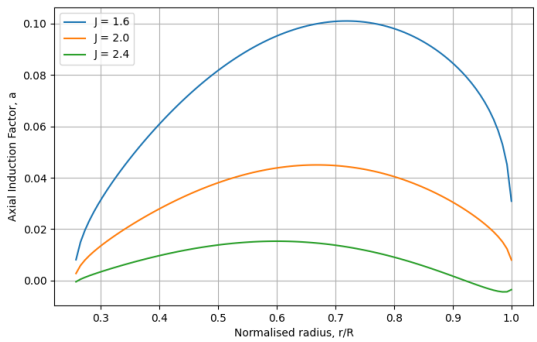

Figure 11: Uncorrected axial induction factor across blade radius

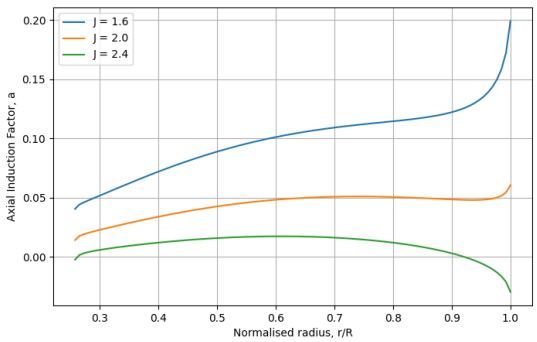

Figure 12: Corrected axial induction factor across blade radius

4.6 Variation of stagnation pressure across blade element at different streamwise locations

In the BEM model developed, the propeller is assumed to be an actuator disk that allows the air to flow continuously through it. This actuator disk is responsible for the pressure jump in the flow. Figure 13 shows the variation of the static pressure, velocity, and stagnation pressure at different streamwise positions according to the actuator disk theory. It can be seen that even though static pressure decreases near the actuator disk, the velocity increases. Since the stagnation pressure is given by

$$P_{stag} = P_{amb} + q_\infty = P_{amb} + \frac{1}{2}\rho V_\infty^2 \tag{13}$$

The stagnation pressure remains constant upwind of the propeller.

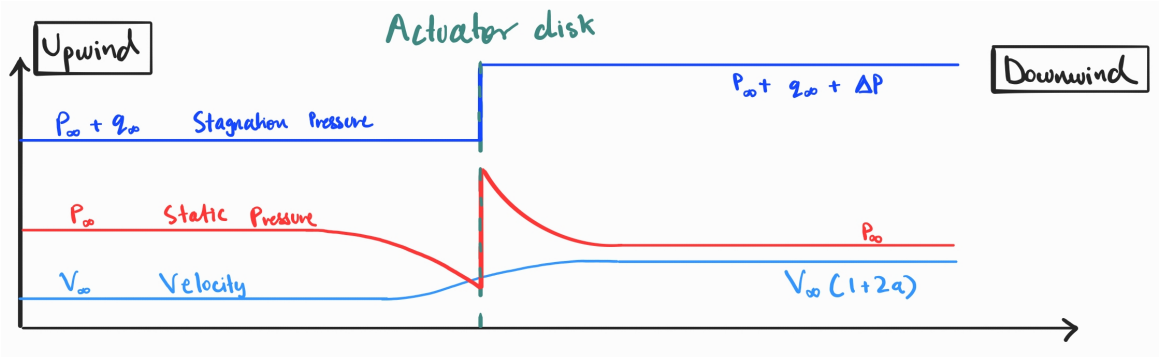

Figure 13: Stagnation Pressure at different streamwise locations

Here, P_{amb} is considered to be the air pressure at 2000 m altitude which is 79.49 KPa, and V_∞ is 60 m/s. Hence, the variation of stagnation pressure across the blade element is the same constant value at the infinity upwind location and at the rotor (upwind side) as seen in Figure 15 and Figure 14. These plots are according to expectations since upwind of the propeller, there is no flow disturbance at both these locations.

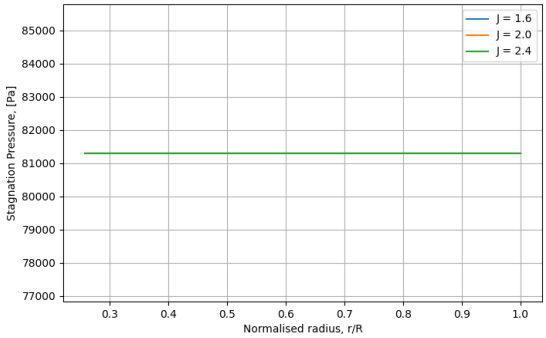

Figure 14: Stagnation Pressure variation at infinity upwind

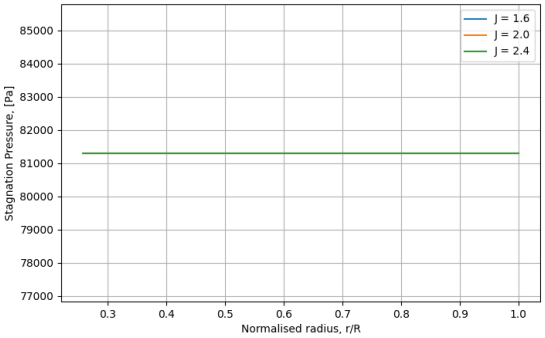

Figure 15: Stagnation pressure variation at the rotor(upwind side)

Again, looking at Figure 13, it can be observed that there is a jump in pressure at the actuator disk. This jump is due to the thrust generated by the actuator disk. The pressure jump is defined as

$$\Delta P = \frac{F_{axial}}{Area} \tag{14}$$

Since the axial force varies for each blade element due to change in local lift and drag of that blade element, the pressure jump varies along the blade location. A radial variation in the stagnation pressure is seen in Figure 16 at the rotor location on the downstream side. A higher stagnation pressure is seen at approximately 0.7 of the normalized radius which indicates that this blade location contributes the most to the thrust generated by the propeller.

At the infinity downstream location (Figure 17), the stagnation pressure variation across the blade radius is the same as the variation for downstream side of the rotor, since there are no external forces to change the flow field (see Figure 13).

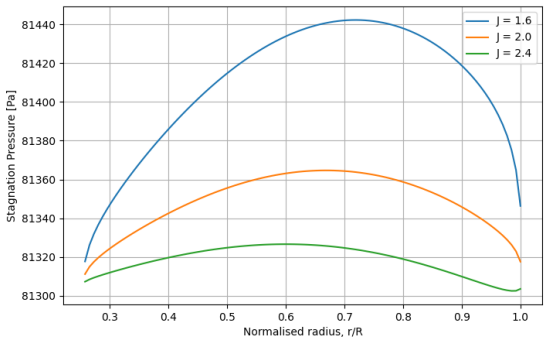

Figure 16: Stagnation pressure variation at the rotor(downwind side)

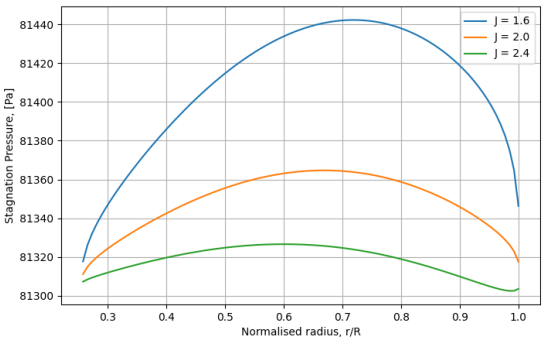

Figure 17: Stagnation Pressure variation at infinity downwind

4.7 Operational point of the airfoil

From the plots in Figure 18, and Figure 19, it can be observed that the highest loaded section is between $55-65\%$ of the span, further implying that sectional lift varies along the blade span. This corroborates the plots obtained for the α variation, Figure 4, and supports the theory and reasoning presented in the preceding sections. The blade L/D also varies along the span. In practical applications, the aerodynamic efficiency, and the load distribution of the rotor blade should be constant along the span to avoid any critical blade section which may limit the operability of the propeller.

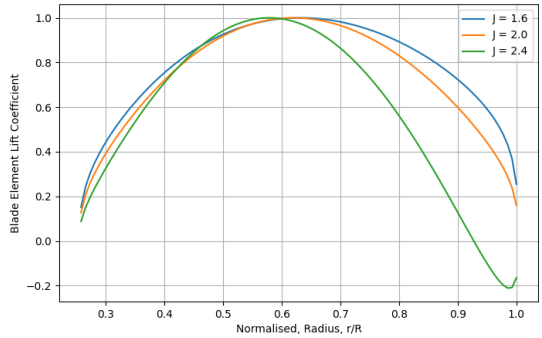

Figure 18: Lift coefficient variation across blade radius

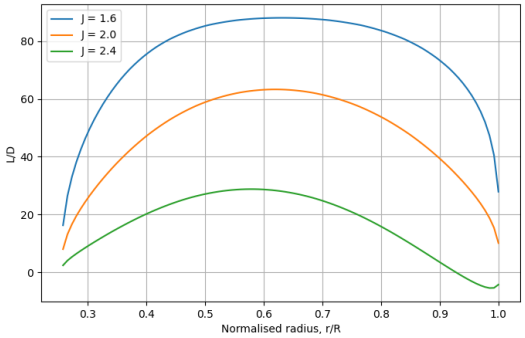

Figure 19: Lift to drag ratio variation across blade radius

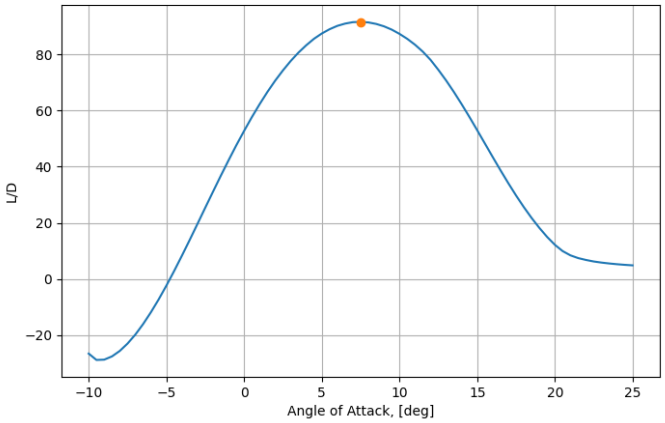

Figure 20: Operational point of the airfoil ARAD-8%.

Figure 20 shows that the most efficient operational point for the airfoil, is at $\alpha \approx 7.5°$. For the propeller blade, it implies that the local angle of attack at each blade section should be about 7.5° in order to have a uniform load distribution along the blade span (as opposed to current load given in Figure 18), and operate at the most optimum aerodynamic point.

5 Conclusion

The BEM model offers a practical way to estimate the aerodynamic performance of a propeller, especially in terms of how thrust and torque vary with operating conditions. From the results, it is clear that increasing advance ratio, decreases both thrust and torque. It also reduces the angle of attack at each blade section, which in turn lowers lift and overall blade loading.

One of the key observations was that a major part of the thrust came from around 55–65% of the blade span. This region corresponded with the highest lift coefficients and inherently highest loading, as can be deduced from Figure 18. If each section of the blade could operate close to the airfoil's optimal angle of attack (around 7.5°), the loading would be more uniform and the blade performance would be more efficient.

Although the model serves as a reliable method for preliminary design, the BEM model has several assumptions for simplification. It assumes that the flow conditions as steady, incompressible, and inviscid, with no radial flow or unsteady effects. These help make the model simpler for solving, however, overlooks the flow physics near the blade root and tip. To account for this, Prandtl's tip and root loss corrections are implemented, and while they improve the induction predictions in those areas, they are still approximations.

While BEM isn't perfect, it is useful in preliminary blade analysis. It is quick, gives reasonable results, and helps in understanding how the propeller behaves under different conditions. Further accuracy can be obtained to correct the limitations, such as the turbulent wake state corrections and the radial flow corrections. For a more detailed understanding of the flow phenomenon, CFD simulations can be used.

6 References

1. Delft University of Technology, "Rotor/Wake Aerodynamics Assignment 1 2024–25", Faculty of Aerospace Engineering, 2024.

2. G. van Kuik, The Fluid Dynamic Basis for Actuator Disc and Rotor Theories. 2018. [Online]. Available: https://doi.org/10.3233/978-1-61499-866-2-i

3. M. K. Rwigema, "Propeller blade element momentum theory with vortex deflection," in Proc. ICAS, ICAS 2010-2.3.3, Nice, France, 2010.

4. "Blade Element Propeller Theory," Aerodynamics for Students. [Online]. Available: https://www.aerodynamics4students.com/propulsion/blade-element-propeller-theory.php

5. E. Branlard, Wind Turbine Aerodynamics and Vorticity-Based Methods: Fundamentals and Recent Applications. Cham, Switzerland: Springer, 2017.